J Mater Sci: Mater Electron (2017) 28:18–27
DOI 10.1007/s10854-016-5488-z

Thermal stability and fire behavior of aluminum diethylphosphinate-epoxy resin nanocomposites

Liqiang Gu[1] · Jianhui Qiu[1] · Eiichi Sakai[1]

Received: 30 May 2016 / Accepted: 2 August 2016 / Published online: 11 August 2016

Abstract The flame retardancy of 2, 2-bis(4-glycidyloxyphenyl)propane (DGEBA)-aluminum diethylphosphinate (AlPi) nanocomposites (EP-AlPi/(P − x), x = 1, 2, 3 %) was greatly enhanced by ultrasonic dispersion of nano-sized AlPi into epoxy resin. The UL 94 V-0 rating can be reached for EP-AlPi nanocomposites with a relatively low addition amount of AlPi (on the account of 8.4 wt% or phosphorus content of 2 wt%) as well as the LOI value over 37.2. The glass transition temperature (T_g) enhanced properties were investigated by DTA, which showed that: T_gs were about 5 °C higher than that of neat epoxy resin; T_g increased along with content increasing of AlPi. Based on TGA results under a non-isothermal condition, the thermal degradation kinetics of EP-AlPi/(P − x) composites were studied by Kissinger's, Ozawa's, Flynn–Wall–Ozawa's and Coast-Redfern's methods, which suggested the conversion function $f(\alpha) = 1/2\alpha^{-1}$ or $f(\alpha) = [-\ln(1-\alpha)]^{-1}$ for EP-AlPi/(P − 1 %); $f(\alpha) = [-\ln(1-\alpha)]^{-1}$ for EP-AlPi/(P − 2 %) and EP-AlPi/(P − 3 %) during the investigated process. The epoxy resin nanocomposites obtained in this study are green functional polymers and will become flame retardant potential candidates in electronic fields such as printed wiring boards with high performance.

1 Introduction

Flame-retardant epoxy resins have been widely applied in electrical laminates and encapsulation resins [1–3], construction materials [4], adhesives [5] and protective coatings [6] due to their safeguard against the potential fire hazard. However, halogen-containing flame-retardant epoxy resins like brominated ones cause serious environmental problems, i.e., the generation of toxic and corrosive fumes during combustion [7–11]. Environment friendly epoxy resins, so called "green flame-retardant epoxy resins", have received considerable attention. Halogen-free flame-retardant (HFFR) epoxy resins as a sustainable replacement for traditional halogen-containing flame-retardant epoxy resins have received growing interest recently because of environmental concerns and end-to-life issues [12–16]. Suihkonen et al. introduced nano- and micro- sized magnesium hydroxide (MDH) into epoxy resin and the results showed that nano-MDH-modified epoxy resins displayed good flame retardancy and mechanical properties with MDH-content of 10 wt% [17]. Such metal (aluminum, magnesium and calcium, etc.) hydroxide flame retardants rapidly gain their market share for their low cost and high performance [18]. Recently, phosphorus-containing flame retardants have been considered to be one of the most high-flame-efficient HFFRs for epoxy resins, as phosphorylation impart significant flame retarding property to epoxy resins [19–23]. In 1980, Cerny et al. [24] reported in U.S. Patent that small amount of red phosphorus as flameproofing agent used in epoxy resin resulted in better mechanical properties and did not interfere with the electrical properties. However, red phosphorus used directly in epoxy resin, suffered from the disadvantage of igniting easily, reacting with moisture in the air, its inherent color and so on. Wang et al. [25] prepared a series of intumescent flame-retardant (IFR) epoxy resins by adding a

Electronic supplementary material The online version of this article (doi:10.1007/s10854-016-5488-z) contains supplementary material, which is available to authorized users.

✉ Jianhui Qiu
qiu@akita-pu.ac.jp

[1] Department of Machine Intelligence and Systems Engineering, Faculty of Systems Science and Technology, Akita Prefectural University, Yurihonjo 015-0055, Japan

5 wt% total loading of ammonium polyphosphate (APP) and metal compounds, which provided UL 94 V-0 classification. Unfortunately, the addition of IFRs generally decreased the mechanical properties of epoxy resin.

Metal salts of dialkylphosphinates, as an important branch of additive-type phosphorus-containing flame retardants, show a high performance in epoxy resin, as well as their high phosphorus content and low addition amount which influence less on the mechanical and electrical properties of epoxy resin [16, 20, 26–30]. Liu et al. compared the flame retardancy and mechanical properties of aluminum diethylphosphinate (Al(DEP) or AlPi) and aluminum methylethylphosphinate (Al(MEP))-filled epoxy composites, and found that both Al(DEP)- and Al(MEP)-modified epoxy resins reached UL 94 V-0 flammability rating at the content of 15 wt% [31]. However, the compatibility and dispersion of such dialkylphosphinate salts with epoxy resin matrix is still a challenge for better flame retardancy and usability mechanical properties.

In this study, nano-sized AlPi was well dispersed into epoxy resin by the long-time ultrasonication technique to form flame-retardant EP-AlPi composites. Such EP-AlPi nanocomposites showed high performance that: meeting UL 94 V-0 flammability rating with AlPi content 8.7 wt% (phosphorus content 2 wt%); LOI values of more than 36; higher T_g (>153.7 °C) than that of neat epoxy resin. Furthermore, thermal degradation kinetic analysis based on Kissinger's, Ozawa's and FWO's methods were taken to describe the thermal degradation behaviors and suggest kinetic parameters (activation energy E and pre-exponential factor A). Coast-Redfern's method suggested the conversion function $f(\alpha) = 1/2\alpha^{-1}$ or $f(\alpha) = [-\ln(1-\alpha)]^{-1}$ for EP-AlPi/(P − 1 %), $f(\alpha) = [-\ln(1-\alpha)]^{-1}$ for EP-AlPi/(P − 2 %) and EP-AlPi/(P − 2 %) during the investigated process to describe the mechanisms of such degradation process.

2 Experimental section

2.1 Materials

4,4′-methylenedianiline (DDM) from Tokyo Chemical Industry Co., Ltd., Japan, was used as received. According to the supplier (Clariant Chemicals Ltd., Germany.), the average particle size for nano-aluminum diethylphosphinate (AlPi) is about 500 nm. It was dried at 80 °C for 12 h in a vacuum oven before adding into epoxy resin. Diglycidyl ether of bisphenol A (DGEBA, E51, epoxy equivalent = 0.51 mol/100 g) was provided by Sinopec, the China Petroleum & Chemical Corporation.

2.2 Preparation of EP-AlPi composites

The AlPi-modified epoxy resins with phosphorus content of 1, 2 and 3 wt% were cured using DDM as hardeners, which were labeled as EP-AlPi/(P − 1 %), EP-AlPi/(P − 2 %) and EP-AlPi/(P − 3 %). Curing procedure: AlPi and Epoxy resin were mixed and stirred by a mechanical stirrer at 20 rpm, accompanied with dispersing through ultrasonication technique (600 W) at 30 °C for 2 h. Then the appropriate amount of DDM (EP/DDM = 100/25, w/w) was added when the mixtures were heated to 100 °C. After degasification, the prepared mixture was poured into the mold. The systems were cured at 140 °C for 2 h and then 180 °C for 2 h. Thereafter, the epoxy thermosets were allowed to cool slowly to room temperature, in order to prevent cracking.

2.3 Instrumental analysis and measurements

FT-IR spectra were recorded on Thermo Scientific Nicolet iN10 MX FT-IR microscope with the optical range of 400–4000 cm^{-1}. The spectra for FT-IR and microstructure observations were sliced using a microtome (RM2145; Leica Microsystems) into 10 μm thickness after being cut from the center of their width. Microstructure was observed in the specimens with a polarized optical microscope (Eclipse model ME600D; Nikon). The bend strength and modulus are measured according to JIS K7171 using a universal testing machine (Series 3360, Instron Co., Ltd., Canton, America) with a bend speed of 2 mm·min^{-1} at 23 ± 1 °C. The scanning electron microscope (SEM) observation was performed on a Hitachi S-4300 scanning electron microscope in high vacuum mode with 5.0 kV acceleration voltage and a medium spot size to investigate the morphologies and distribution of the AlPi in epoxy resin. Thermal gravimetric analyses (TGA) of samples were carried out with Shimadzu DTG-60/60H from 50 to 600 °C at heating rates of 5, 10, 15, and 20 °C·min^{-1}, whereas the flow of nitrogen or air was maintained at 50 mL·min^{-1}. Differential thermal analysis (DTA) were taken with the same instrument from 50 to 200 °C at heating rates of 5 °C·min^{-1}. The Underwriter Laboratories 94 vertical tests (UL 94) were performed according to IEC 60695-11-10:1999 using a horizontal and vertical burning instrument (FZ-5401, Dongguan Hanyang electronic instrument Co., Ltd, China). The LOI test was performed according to the testing procedure of ISO 4589-2:1996 with the dimensions 80 × 6 × 3 mm^3 of each sample.

3 Results and discussion

3.1 Characterization and dispersion of the AlPi in epoxy resin

The morphologies and dispersion of additive-type flame retardant in epoxy resin plays an important role in mechanical properties as well as flame retardancy. Figure 1 shows the FT-IR spectra of AlPi, EP-AlPi/(P − 1 %), EP-AlPi/(P − 2 %) and EP-AlPi/(P − 3 %). The appearance of P–O stretching vibration at 780 cm^{-1} for EP-AlPi/(P − 1 %), EP-AlPi/(P − 2 %) and EP-AlPi/(P − 3 %) demonstrates that the mix of AlPi into epoxy resin, where infrared transmittance decrease following the increasing of AlPi content. The peaks at 1610 and 1500 cm^{-1} are ascribed to N–H bending vibration and aromatic ring skeleton vibration corresponds to curing agent DDM and diglycidyl ether of bisphenol A. To further investigate the dispersion of AlPi in epoxy resin, FT-IR spectra of EP-AlPi/(P − 3 %) were taken under the line mapping model. In Fig. 2a, we evaluate the spatial resolution and reproducibility of FTIR spectroscopy by recording spectra along the red line in the topography image (Fig. 2b). Such spectral mapping scan reveals the N–H bending vibration peak (1610 cm^{-1}) from inside of the membrane until the edge is reached, while the tip is scanning in steps of 100 μm from inside to surface. Plotting the FT-IR transmission at 780 and 1500 cm^{-1} as a function of AlPi and epoxy resin at the fifteen Y-positions (red dot in Fig. 2b) show the same of transmission peaks. We further note that the inside fourteen infrared spectra on the Y-positions exhibit a stable peak position and peak height, which illustrates the high reproducibility of FTIR (Fig. 2c). On the other hand, the stable ratios of peak height at 780 and 1500 cm^{-1} show that different positions of such AlPi-epoxy nanocomposites exhibit constant AlPi content, confirming a well dispersion of AlPi in epoxy resin, which is an improvement by the long-time ultrasonication technique.

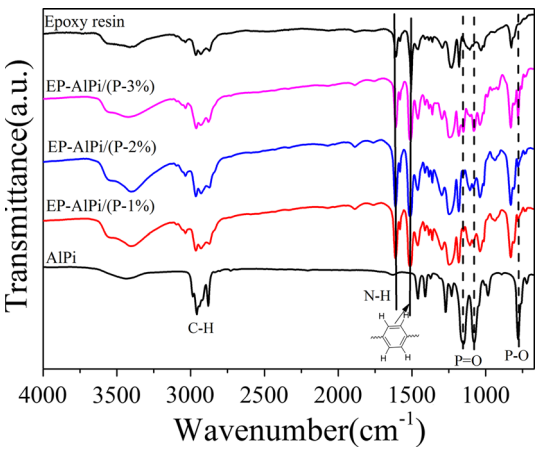

Fig. 1 FT-IR spectra of AlPi, EP-AlPi/(P − 1 %), EP-AlPi/(P − 2 %) and EP-AlPi/(P − 3 %)

Figure 3 shows polarizing optical micrograph of EP-AlPi/(P − 1 %), EP-AlPi/(P − 2 %) and EP-AlPi/(P − 3 %). It is obviously that there are no clearly bulk aggregates of AlPi in EP-AlPi/(P − 1 %) nanocomposites (Fig. 3a), which shows well dipersibility of AlPi in epoxy resin because that long-time ultrasonication before curing process improve the dispersibility of filler in epoxy resin. Therefore, the bending strength and flexural modulus of EP-AlPi/(P − 1 %) keep unchanged to pure epoxy resin as shown in mechanical properties. As AlPi contents doubling, about 5 μm white AlPi-balls spread out evenly into the whole epoxy matrix (Fig. 3b, c). This can be attribute to the poor chemical combination of AlPi to epoxy resin, which is the common drawback of all additive-type flame retardants.

3.2 Mechanical properties

To identify the effect of filler content on mechanical properties of AlPi-epoxy nanocomposites, the weight fraction of nano-AlPi in epoxy was varied from 4.2 to 12.6 % (or phosphorus content from 1 to 3 %). Stress–strain curves obtained from the flexural tests are shown in Fig. 4a. All the four stress–strain curves showed considerable non-linearity before reaching the ultimate strength. Most of the samples failed immediately after reaching their ultimate strength. However, we can find that maximum strains increase with the content of AlPi increasing. Average and standard deviation values of bending strength and flexural modulus obtained from these tests are shown in Fig. 4b. It can be observed in Fig. 4b that both bending strength and flexural modulus slightly decrease along with the addition of AlPi, whereas EP-AlPi/(P − 3 %) with AlPi content 12.6 wt% shows higher bending strength than EP-AlPi/(P − 2 %). These results indicate that mixing AlPi and epoxy resin with long-time ultrasonication helps to break the agglomeration of AlPi which affects the usability mechanical properties of those nanocomposites.

Figure 5 shows SEM images of the fracture surfaces from impact specimens with (a) EP-AlPi/(P − 1 %), (b) EP-AlPi/(P − 2 %) and (c) EP-AlPi/(P − 3 %) according with AlPi-content of 4.2, 8.4 and 12.6 wt%, respectively (Table 1). It is obvious that there are no clearly bulk aggregates of AlPi in EP-AlPi nanocomposites (Fig. 5), which shows well dispersibility of AlPi in epoxy resin because of the long-time ultrasonication technique. However, with the AlPi content increasing, the AlPi-ball

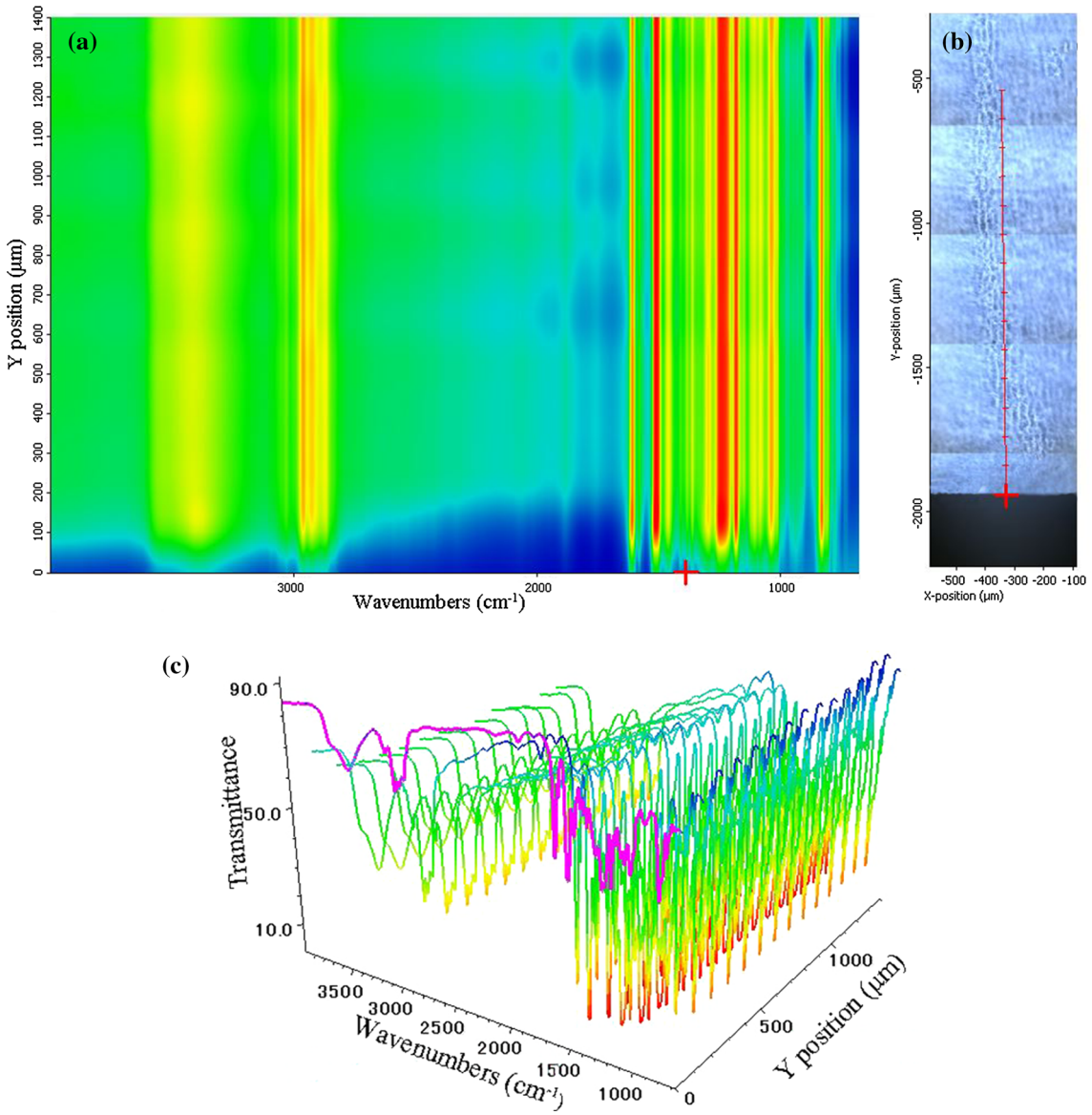

Fig. 2 FT-IR spectra of EP-AlPi/(P − 3 %) under line mapping model: **a** the contour line image, **b** topography image and **c** 3-D FT-IR spectra

can be observed (Fig. 5b, c.) because of its poor chemical combination to epoxy resin. For low AlPi loading composites (EP-AlPi/(P − 1 %), Fig. 5a), the smooth surface indicates a brittle fracture. While, for higher AlPi content composites, rougher surfaces are generated with small and dense bulk, which also can be attributed to the poor chemical combination.

3.3 Flammability and thermal stability

The flame-retardant performance of the EP-AlPi composites have been investigated in terms of UL-94 vertical burning tests, and the results are summarized in Table 1. It is clear that UL 94 V-0 flammability rating can be reached for EP-AlPi/(P − 2 %) (on the AlPi-account of 8.4 wt%) and meanwhile the LOI value reached over 37.2. The flame retardancy of EP-AlPi/(P − x) thermosets increases with the phosphorus content increasing. When 4.2 wt% AlPi is added, the LOI value of EP-AlPi/(P − 1 %) is increased to 36, however, this sample can reach only UL 94 V-1 rating. EP-AlPi/(P − 3 %) with 12.6 wt% AlPi addition achieves a higher LOI value of 39.5 and the UL 94 V-0 rating. According to the above results, a significant improvement of the flame retardancy for those nanocomposites by well dispersion of nano-AlPi into epoxy resin.

The thermal stability of epoxy resin and EP-AlPi composites were investigated by TGA and DTA under nitrogen atmospheres at heating rates of 5, 10, 15 and 20 °C·min^{-1}. The TGA curves under nitrogen and air atmospheres are respectively shown in Fig. 6, and the analysis results are

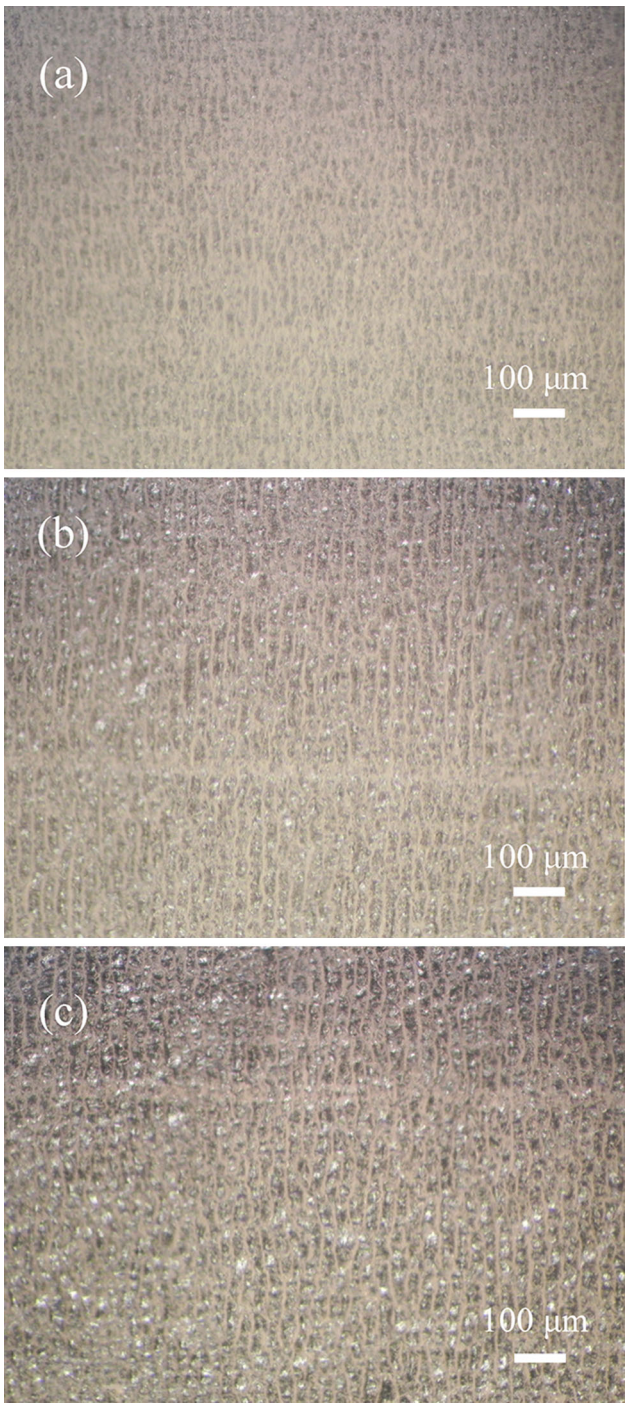

Fig. 3 Polarizing optical micrograph of **a** EP-AlPi/(P − 1 %), **b** EP-AlPi/(P − 2 %) and **c** EP-AlPi/(P − 3 %)

summarized in Table 1. Under nitrogen atmospheres, there is only a one-sharp weight loss stage for all the samples (Fig. 6a). The onset decomposition temperature of 5 % weight loss ($T_{5\%}$) at a heating rate of 10 °C·min^{-1} is 365.62, 363.32 and 364.55 °C for EP-AlPi/(P − 1 %), EP-AlPi/(P − 2 %) and EP-AlPi/(P − 3 %), respectively, significantly lower than that (377.79 °C) of epoxy resin (Inside of Fig. 6a). The decreasing trend of $T_{5\%}$ can be attributed to the fact that the O=P–O bond in AlPi-modified epoxy resin is more active than common C–C bond, which is also suggested to form phosphorus-containing radical stabilizers by the quenching mechanism in combustion. Additionally, EP-AlPi composites show slower weight loss rate than that of neat epoxy resin. It is noteworthy that higher char yield can be obtained accompany with the addition of AlPi, as charring layer plays a very important role in the performance of flame retardancy.

TG and curves of epoxy resin and EP-AlPi composites in the air condition are also shown in Fig. 6. The EP-AlPi composites show two-stage decomposition processes, which presents a significantly different thermal behavior in the air condition compared to that in the nitrogen condition. It shows a slower weight decrease process between 350 and 375 °C in the air condition. When the temperature further increases, those EP-AlPi composites show another decrease of mass start from 530 °C, whereas the char residue at 600 °C is higher than that under nitrogen condition. These different may be attribute to the different degradation behavior of AlPi in air condition [31].

Figure 7 shows DTA thermograms of epoxy resin and AlPi-modified epoxy thermosets. Obtained from that, T_gs are summarized in Table 1. It is expected that all EP-AlPi composites show a high-T_g over 153.7 °C, higher than that (148.5 °C) of neat epoxy resin, indicating an excellent thermal stability for AlPi-modified epoxy thermosets. Moreover, T_g-enhanced properties are found following the T_g-increased trend with AlPi-content increasing.

3.4 Kinetic analysis

According to the TGA curves of AlPi-modified epoxy thermosets shown in Figure S4, the thermal kinetics of the EP-AlPi composites were studied by Kissinger's [32], Ozawa's [33] and FWO's [34] methods under a non-isothermal condition.

In the case of Kissinger's method, the activation energy (E_K) can be given from the slope of the plot of ln (β/T_p^2) versus $1/T_p$ by the equation as follows:

$$\ln\left(\beta/T_p^2\right) = -E_K/RT_p + \ln(AR/E_K) \quad (1)$$

where β is the heating rate (K·min^{-1}), T_p is the peak temperature at the heating rate of β, A is the frequency factor (s^{-1}), E_K is the activation energy of curing reaction (kJ mol^{-1}), R is the gas constant (8.314 J·K^{-1}·mol^{-1}).

Figure 8 illustrates the Kissinger's plots of EP-AlPi composites. The thermal decomposition kinetic parameters, i.e., E_K and A, are summarized in Table 2.

Furthermore, the activation energy (E_O) derived from Ozawa's method can also be obtained from the slope of the

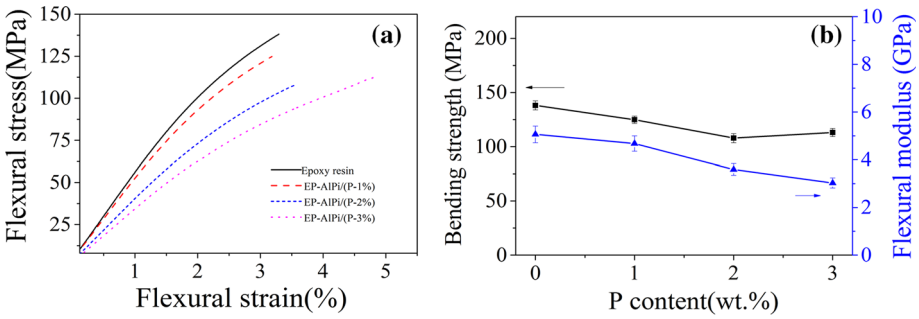

Fig. 4 **a** Flexural strain–stress curves, **b** bending strength and flexural modulus of Epoxy resin, EP-AlPi/(P − 1 %), EP-AlPi/(P − 2 %) and EP-AlPi/(P − 3 %)

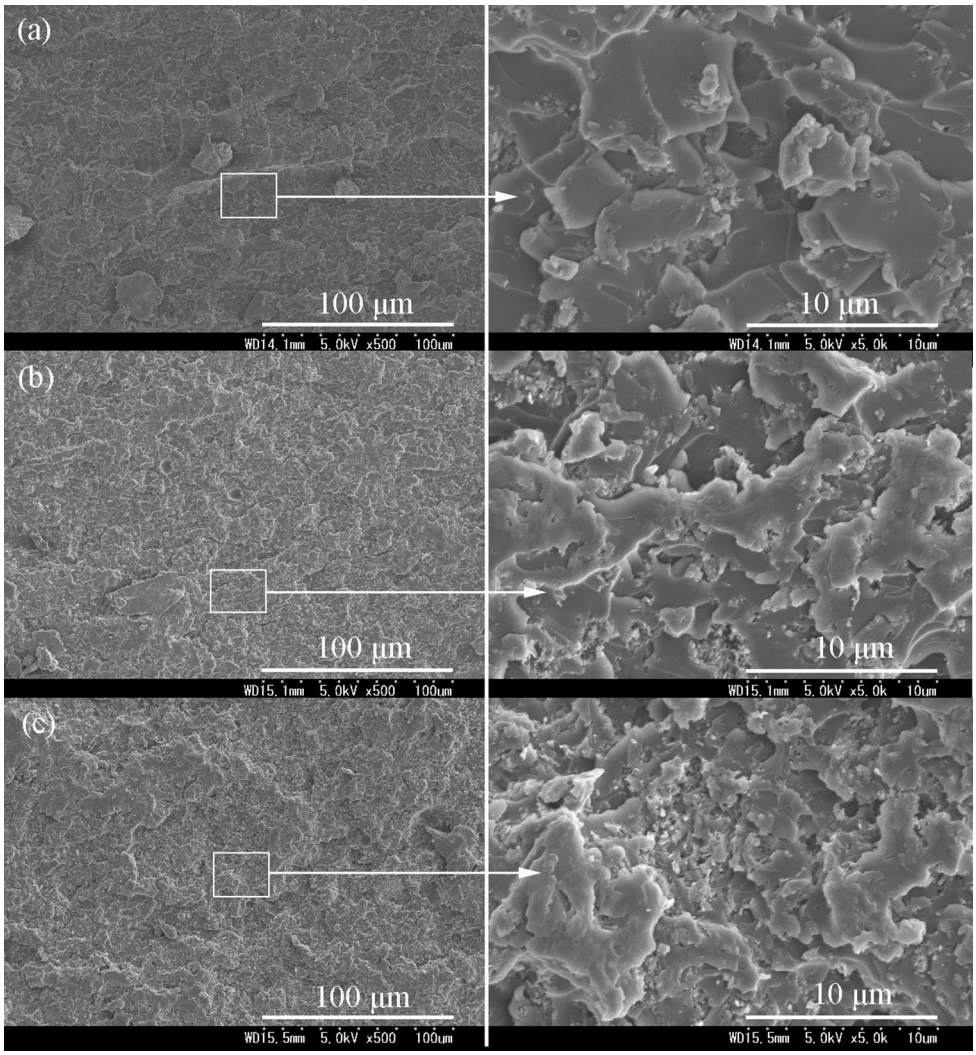

Fig. 5 SEM images of fractographs from the impact test specimen of AlPi-modified epoxy thermosets **a** EP-AlPi/(P − 1 %), **b** EP-AlPi/(P − 2 %), **c** EP-AlPi/(P − 3 %)

plot of ln β versus $1/T_p$ according to the Ozawa's equation expressed as follows:

$$\ln \beta = -1.052E_O/RT_p + \ln(AE_O/R) - 5.331 \quad (2)$$

Figure 9 shows the linear fitting curves of AlPi-modified epoxy thermosets using Ozawa's methods. The obtained results such as E_O and A_O are summarized in Table 2.

It can be observed that E_K and E_O show a good agreement for each EP-AlPi composites. The values of E_K and E_O for these three AlPi-content epoxy thermosets exhibit a variation trend in an order of EP-AlPi/(P − 1 %) > EP-AlPi/(P − 2 %) > EP-AlPi/(P − 3 %). This means the thermal decomposition process starts earlier as well as higher AlPi-content, corresponding with decreasing trend of $T_{5\%}$.

Flynn–Wall–Ozawa's (FWO's) method is expressed as Eq. (3):

$$\lg \beta = -0.4567E_F/RT + \lg(AE_F/Rg(\alpha)) - 2.315 \quad (3)$$

Table 1 Thermal and flame-retardancy properties of epoxy thermosets

Thermoset ID	AlPi (wt%)[a]	P (wt%)[b]	T_g (°C)[c]	Char yield[d]	Char yield[e]	UL-94 grade	LOI
Epoxy resin	0	0	148.5	21	20.6	No rating	25
EP-AlPi/(P − 1 %)	4.2	1	153.7	20.7	20.3	V-1	36
EP-AlPi/(P − 2 %)	8.4	2	154.9	22.1	24.1	V-0	37.2
EP-AlPi/(P − 3 %)	12.6	3	156.3	24.2	25.4	V-0	39.5

[a] (wt%) Flame retardant content

[b] (wt%) Phosphorus content

[c] (°C) Measured by DTA

[d] (wt%) Residual weight percentage at 600 °C with heating rate of 10 °C·min^{-1} in nitrogen atmosphere

[e] (wt%) Residual weight percentage at 600 °C with heating rate of 10 °C·min^{-1} in air atmosphere

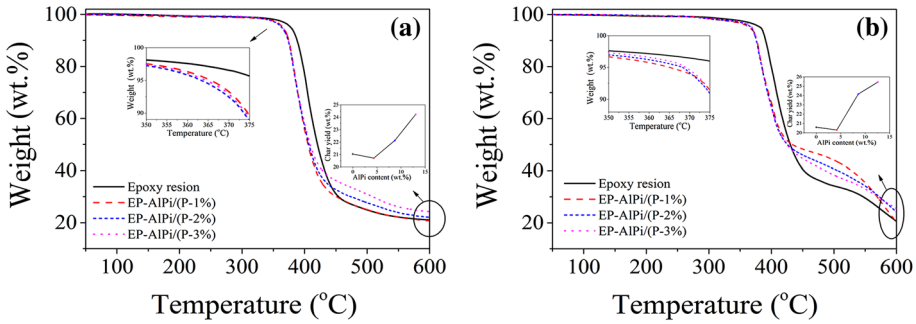

Fig. 6 TGA curves of the thermal decomposition of epoxy resin and epoxy systems with EP-AlPi/(P − 1 %), EP-AlPi/(P − 2 %), EP-AlPi/(P − 3 %) under **a** nitrogen atmospheres, **b** air atmospheres at a heating rate of 10 °C·min^{-1}

By FWO's method (Fig. 10), taking degree of conversion (α) from 10 to 90 %, the activation energy (E_F) at different percentage of α can be obtained from the slope of the plot of lg β versus $1/T_p$. The average E_F are summarized in Table 2. It can be seen that EP-AlPi/(P − 2 %) and EP-AlPi/(P − 3 %) have two sets of parallel lines, which means two stages for these two samples. The average values of EP-AlPi/(P − 2 %) are 160.44 (α = 0.1–0.7) and 245.93 (α = 0.8–0.9) kJ·mol^{-1}, and the E_F values of EP-AlPi/(P − 3 %) are 147.09 (α = 0.1–0.6) and 244.42 (α = 0.7–0.9) kJ·mol^{-1}, respectively, as shown in Table 2.

However, for all the samples, the average E_F(s) of the first stage show good agreements with E_K(s) and E_O(s), in an order of Epoxy resin > EP-AlPi/(P − 1 %) > EP-AlPi/(P − 2 %) > EP-AlPi/(P − 3 %). As shown in Fig. 10, the change of E_F(s) at different conversion degree indicates complex decomposition mechanisms of flame-retardant EP-AlPi composites.

Adopting the above activation energy (E_K, E_O and E_F) and frequency factor (A_K, A_O and A_F), the most probable mechanism function (MPMF) can be obtained based on Eq. (4) deduced from Coast-Redfern's method [35]:

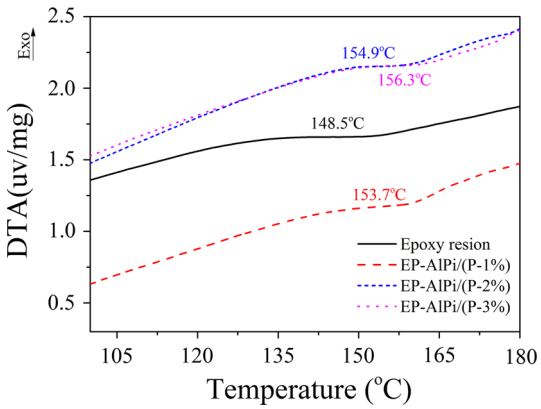

Fig. 7 DTA for AlPi-modified epoxy systems with various phosphorus-content of 0, 1, 2 and 3 wt%

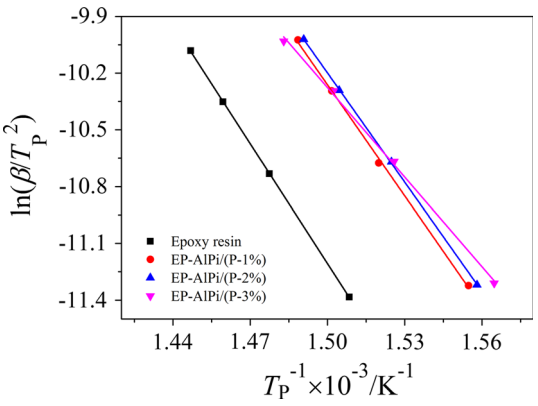

Fig. 8 Kissinger's plots of AlPi-modified epoxy systems with various phosphorus-content of 0, 1, 2 and 3 wt%

Table 2 Thermal decomposition kinetic parameters derived from Kissinger's, Ozawa's and FWO's method

Thermoset ID	Kissinger method		Ozawa method		FWO method
	E_K (kJ·mol^{-1})	lnA_K	E_O (kJ·mol^{-1})	lnA_O	av. E_F (kJ·mol^{-1})
Epoxy resin	175.57	23.52	177.58	37.77	172.58
EP-AlPi/(P − 1 %)	162.71	22.07	165.05	36.41	162.08 (0.1 ~ 0.8)
EP-AlPi/(P − 2 %)	160.03	21.63	162.48	36.00	160.44 (0.1 ~ 0.7), 245.93 (0.8 ~ 0.9)
EP-AlPi/(P − 3 %)	131.14	16.14	135.03	30.90	147.09 (0.1 ~ 0.6), 244.42 (0.7 ~ 0.9)

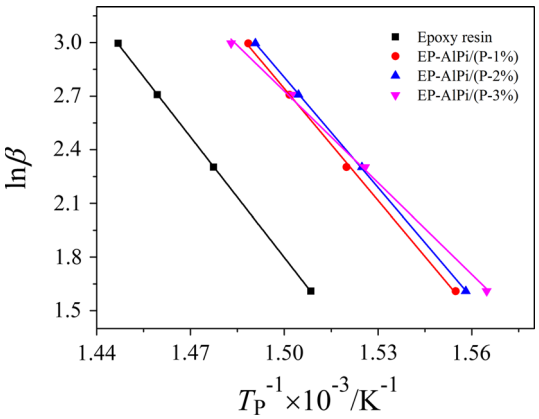

Fig. 9 Ozawa's plots of AlPi-modified epoxy systems with various phosphorus-content of 0, 1, 2 and 3 wt%

$$\ln\left(G(\alpha)/T^2\right) = -E_C/RT + \ln\left(AR/\beta E_C\right) \quad (4)$$

where α is conversion degree, T is corresponding temperature acquired from the TGA curves (Figure S4), G (α) denote fourteen mechanism functions (listed Table S2) [36]. Thus, using a linear regression of least-square method over a large range of conversion (20 % ≤ a ≤ 70 %), four sets of A and E for one sample can be calculated by plots of ln (G (α)/T^2) versus 1000/T with four heating rates (β), respectively (Fig. 11, and S5). Two hundred and twenty-four sets of A and E values for epoxy resin and EP-AlPi/(P − x) thermosets can be obtained by the Coast-Redfern's method. The restrictive conditions for choosing the MPMFs are: E_C of different heating rate approximate to the invariant activation energy E_K, E_O and E_F; the average E_C meets the condition of $|(E_C - E_K)/E_K| \le 0.1$; pre-exponential factor A_K comply with $|(\ln A_C - \ln A_K)/\ln A_K| \le 0.1$; FWO's method with the chosen convention function G (α) can get appreciate A_F comply with $|(\ln A_F - \ln A_K)/\ln A_K| \le 0.2$; all data show well linear correlation (Table S3-S6) [37–40]. According to above conditions, the MPMFs for epoxy resin and EP-AlPi/(P − x) thermosets are chosen and listed in Table 3. From these results, the thermal degradation mechanism of EP-AlPi/(P − 1 %) is expressed as function No. 11 $G(\alpha) = \alpha^2$ (or $f(\alpha) = 1/2\alpha^{-1}$) with

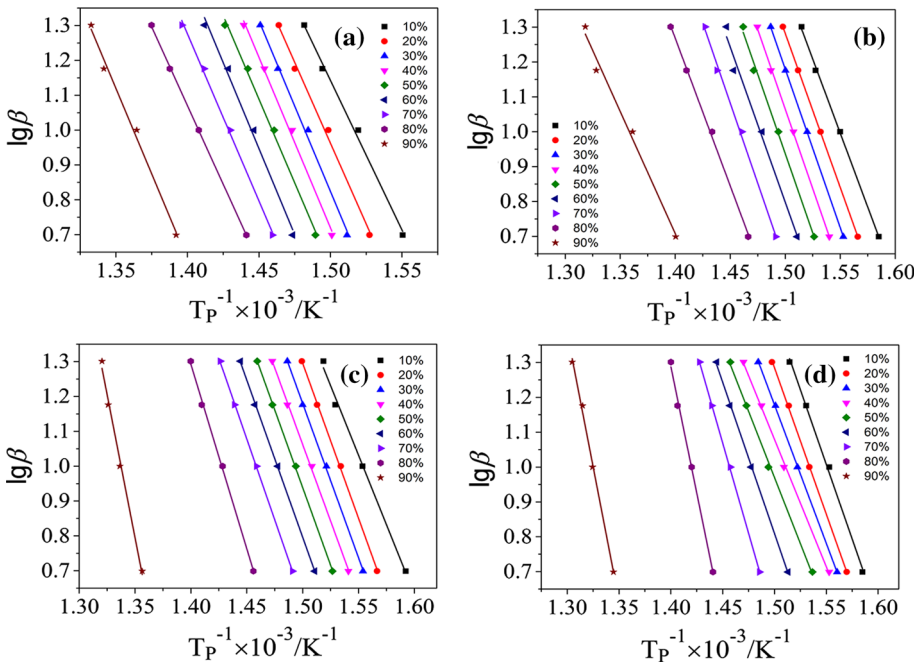

Fig. 10 FWO's plots for **a** epoxy resin and AlPi-modified epoxy systems with **b** EP-AlPi/(P − 1 %), **c** EP-AlPi/(P − 2 %) and **d** EP-AlPi/(P − 3 %)

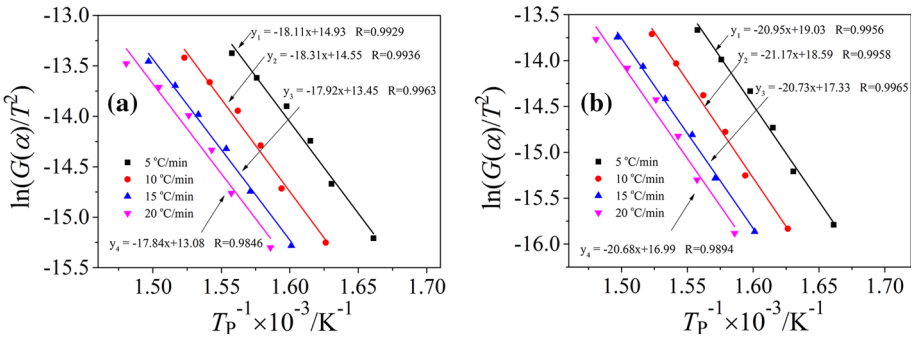

Fig. 11 Coast-Redfern's plots of EP-AlPi/(P − 1 %) with mechanism function of **a** no. 11 and **b** no. 12

Table 3 Expressions of the most probable mechanism functions and kinetic models for epoxy resin and AlPi-modified epoxy resin

Thermoset ID	Code	Model	$f(\alpha)$	$G(\alpha)$	Mechanism
Epoxy resin	D1	Parabolic law	$1/2\alpha^{-1}$	α^2	One-dimensional diffusion, 1D, D_1- deceleration shaped α–t curve
EP-AlPi/(P − 1 %)	D1	Parabolic law	$1/2\alpha^{-1}$	α^2	
	D2	Valensi equation	$[-\ln(1-\alpha)]^{-1}$	$(1-\alpha)\ln(1-\alpha)+\alpha$	Two-dimensional diffusion, cylindrical symmetry, 2D, D_2- deceleration shaped α–t curve
EP-AlPi/(P − 2 %) and EP-AlPi/(P − 3 %)	D2	Valensi equation	$[-\ln(1-\alpha)]^{-1}$	$(1-\alpha)\ln(1-\alpha)+\alpha$	

the mechanism of "One-dimensional diffusion, 1D, D_1-deceleration shaped α–t curve", or function No. 12 $G(\alpha) = (1-\alpha)\ln(1-\alpha)+\alpha$ (or $f(\alpha) = [-\ln(1-\alpha)]^{-1}$) with the mechanism of "Two-dimensional diffusion, cylindrically symmetric, 2D, D_2-deceleration shaped α–t curve". It is interestingly observed from Table 3 that mechanism changed from one-dimensional diffusion to two-dimensional diffusion with AlPi increasing, indicating the complicatedly effect of AlPi on epoxy resin matrix. On the basis of the above thermal degradation kinetic analysis, as the kinetic parameters and the conversion function change, it is concluded that AlPi plays an important role in the thermal degradation process as well as the combustion process.

4 Conclusions

Nano-sized aluminum diethylphosphinate (AlPi) was well dispersed into epoxy resin by the long-time ultrasonication technique to form flame-retardant EP-AlPi nanocomposites. Their flame retardancy-enhanced properties were indicated that EP-AlPi composites with a relatively low addition amount of AlPi (on the account of 8.7 wt% or phosphorus content of 2 wt%) can reach the UL 94 V-0 flammability rating. Moreover, according to the DTA results, AlPi-epoxy thermosets showed a high thermal resistance due to their high T_g over 153.7 °C. Thermal degradation kinetic analysis based on Kissinger's and Ozawa's methods suggested a decreasing trend of the activation energy E, from 165 to 131 kJ·mol^{-1} with AlPi-content from 4.2 to 12.6 %. The isoconversional methods (Kissinger's, FWO's and Coast-Redfern's methods) suggested the F40 conversion function $f(\alpha) = 1/2\alpha^{-1}$ or $f(\alpha) = [-\ln(1-\alpha)]^{-1}$ for EP-AlPi/(P − 1 %); $f(\alpha) = [-\ln(1-\alpha)]^{-1}$ for EP-AlPi/(P − 2 %) and EP-AlPi/(P − 3 %) during the investigated process. The epoxy resin nanocomposites obtained in this study will be potential candidates as green functional materials for flame retardant applications in electronic fields with more safety and high performance.

References

1. D. Sun, Y. Yao, Synthesis of three novel phosphorus-containing flame retardants and their application in epoxy resins. Polym. Degrad. Stab. **96**(10), 1720–1724 (2011)
2. C.S. Wang, J.Y. Shieh, Synthesis and properties of epoxy resins containing 2-(6-oxid-6H-dibenz < c, e > < 1, 2 > oxaphosphorin-6-yl) 1, 4-benzenediol. Polymer **39**(23), 5819–5826 (1998)
3. S.V. Levchik, E.D. Weil, Thermal decomposition, combustion and flame-retardancy of epoxy resins—a review of the recent literature. Polym. Int. **53**(12), 1901–1929 (2004)
4. L.J. Qian, L.J. Ye, G.Z. Xu et al., The non-halogen flame retardant epoxy resin based on a novel compound with phosphaphenanthrene and cyclotriphosphazene double functional groups. Polym. Degrad. Stab. **96**(6), 1118–1124 (2011)

5. J.Y. Shieh, C.S. Wang, Synthesis of novel flame retardant epoxy hardeners and properties of cured products. Polymer **42**(18), 7617–7625 (2001)
6. J. Gu, G. Zhang, S. Dong et al., Study on preparation and fire-retardant mechanism analysis of intumescent flame-retardant coatings. Surf. Coat. Technol. **201**(18), 7835–7841 (2007)
7. J. Sun, X. Wang, D. Wu, Novel spirocyclic phosphazene-based epoxy resin for halogen-free fire resistance: synthesis, curing behaviors, and flammability characteristics. ACS Appl. Mater. Interfaces **4**(8), 4047–4061 (2012)
8. B. Sood, M. Pecht, Conductive filament formation in printed circuit boards: effects of reflow conditions and flame retardants. J. Mater. Sci. Mater. Electron. **22**(10), 1602–1615 (2011)
9. P. Fisk, A. Girling, R. Wildey, *Prioritisation of Flame Retardants for Environmental Risk Assessment* (Environment Agency, Wallingford, 2003)
10. X. Li, Y. Ou, Y. Shi, Combustion behavior and thermal degradation properties of epoxy resins with a curing agent containing a caged bicyclic phosphate. Polym. Degrad. Stab. **77**(3), 383–390 (2002)
11. M. Iji, Y. Kiuchi, Flame resistant glass-epoxy printed wiring boards with no halogen or phosphorus compounds. J. Mater. Sci. Mater. Electron. **15**(3), 175–182 (2004)
12. J. Xu, J. Liu, K. Li, Application of functionalized graphene oxide in flame-retardant polypropylene. J. Vinyl Addit. Technol. **21**(4), 278–284 (2015)
13. M. Iji, Y. Kiuchi, Self-extinguishing epoxy molding compound with no flame-retarding additives for electronic components. J. Mater. Sci. Mater. Electron. **12**(12), 715–723 (2001)
14. X. Li, Y. Liu, C. Guo, H. Liu, G. Wang, Q. Cai, Y. Yao, Influence of layered aluminoborophosphate on flame retardance, crystallization behaviors and mechanical properties of polyamide 66 systems. Chem. Res. Chin. Univ. **32**(1), 127–133 (2016)
15. S.Y. Lu, I. Hamerton, Recent developments in the chemistry of halogen-free flame retardant polymers. Prog. Polym. Sci. **27**(8), 1661–1712 (2002)
16. J. Xu, X. Zhou, C. Ye et al., Thermal stability and mechanical property of polyvinyl chloride/intercalated hydrotalcite. J. Chin. Ceram. Soc. **41**(4), 516–520 (2013)
17. B.I. Noh, S.B. Jung, Characteristics of environmental factor for electrochemical migration on printed circuit board. J. Mater. Sci. Mater. Electron. **19**(10), 952–956 (2008)
18. M. Wang, J. Xu, H. Wu et al., Effect of pentaerythritol and organic tin with calcium/zinc stearates on the stabilization of poly (vinyl chloride). Polym. Degrad. Stab. **91**(9), 2101–2109 (2006)
19. L. Xiao, D. Sun, T. Niu et al., Syntheses and characterization of two novel 9, 10-dihydro-9-oxa-10-phosphaphenanthrene-10-oxide-based flame retardants for epoxy resin. High Perform. Polym. **26**(1), 52–59 (2014)
20. K. Ramachandran, W.J. Ready, P.M. Raj et al., Insulation reliability of fine-pitch through-vias in glass fiber reinforced halogen-free epoxy substrates. J. Mater. Sci. Mater. Electron. **25**(4), 1687–1695 (2014)
21. C.S. Wu, Y.L. Liu, Y.S. Chiu, Epoxy resins possessing flame retardant elements from silicon incorporated epoxy compounds cured with phosphorus or nitrogen containing curing agents. Polymer **43**(15), 4277–4284 (2002)
22. T. Ohki, Q.Q. Ni, N. Ohsako et al., Mechanical and shape memory behavior of composites with shape memory polymer. Compos. A Appl. Sci. Manuf. **35**(9), 1065–1073 (2004)
23. B.I. Noh, N.C. Park, W.S. Hong et al., Effect of underfill on bending fatigue behavior of chip scale package. J. Mater. Sci. Mater. Electron. **19**(5), 406–410 (2008)
24. J. Cerny, G. Vivant, U.S. Patent No. 4,188,313 (U.S. Patent and Trademark Office, Washington, DC), 12 Feb 1980
25. J.S. Wang, Y. Liu, H.B. Zhao et al., Metal compound-enhanced flame retardancy of intumescent epoxy resins containing ammonium polyphosphate. Polym. Degrad. Stab. **94**(4), 625–631 (2009)
26. Z. Yang, C. Zhou, H. Yang et al., Improvement of the compatibilization of high-impact polystyrene/magnesium hydroxide composites with partially sulfonated polystyrene as macromolecular compatibilizers. Ind. Eng. Chem. Res. **51**(27), 9204–9212 (2012)
27. G.H. Hsiue, Y.L. Liu, J. Tsiao, Phosphorus-containing epoxy resins for flame retardancy V: synergistic effect of phosphorus-silicon on flame retardancy. J. Appl. Polym. Sci. **78**(1), 1–7 (2000)
28. C.L. Gan, U. Hashim, Evolutions of bonding wires used in semiconductor electronics: perspective over 25 years. J. Mater. Sci. Mater. Electron. **26**(7), 4412–4424 (2015)
29. T. Niu, D. Sun, Y. Yao, Study on synthesis and application of two phosphorus nitrogen flame retardants for epoxy resin. Plast. Sci. Technol. **41**(4), 107–110 (2013)
30. L. Qian, L. Ye, Y. Qiu et al., Thermal degradation behavior of the compound containing phosphaphenanthrene and phosphazene groups and its flame retardant mechanism on epoxy resin. Polymer **52**(24), 5486–5493 (2011)
31. W.P.S. Saw, M. Mariatti, Properties of synthetic diamond and graphene nanoplatelet-filled epoxy thin film composites for electronic applications. J. Mater. Sci. Mater. Electron. **23**(4), 817–824 (2012)
32. H.E. Kissinger, Reaction kinetics in differential thermal analysis. Anal. Chem. **29**(11), 1702–1706 (1957)
33. T. Ozawa, A new method of analyzing thermogravimetric data. Bull. Chem. Soc. Jpn. **38**(11), 1881–1886 (1965)
34. J.H. Flynn, L.A. Wall, A quick, direct method for the determination of activation energy from thermogravimetric data. J. Polym. Sci. Part C Polym. Lett. **4**(5), 323–328 (1966)
35. A.W. Coats, J.P. Redfern, Kinetic parameters from thermogravimetric data. Nature **201**, 68–69 (1964)
36. S. Vyazovkin, K. Chrissafis, M.L. Di Lorenzo et al., ICTAC kinetics committee recommendations for collecting experimental thermal analysis data for kinetic computations. Thermochim. Acta **590**, 1–23 (2014)
37. R.Z. Hu, S.L. Gao, F.Q. Zhao, Q.Z. Shi, T.L. Zhang, J.J. Zhang, *The Foundation of Modern Chemisty Series Book 14: Thermal Analysis Kinetic* (Science Press, Peking, 2008), pp. 54–176
38. K. Pielichowska, Thermooxidative degradation of poly-oxymethylene homo-and copolymer nanocomposites with hydroxyapatite: kinetic and thermoanalytical study. Thermochim. Acta **600**, 7–19 (2015)
39. D. Yang, Y. Hu, H. Li, L. Song, H. Xu, B. Li, Synergistic flame retardant effect of α-zirconium phosphate in low-density polyethylene/ethylene-vinyl acetate/aluminum hydroxide hybrids. J. Therm. Anal. Calorim. **119**(1), 619–624 (2015)
40. J. Xu, Z. He, W. Wu et al., Study of thermal properties of flame retardant epoxy resin treated with hexakis [p-(hydroxymethyl) phenoxy] cyclotriphosphazene. J. Therm. Anal. Calorim. **114**(3), 1341–1350 (2013)